Development of a Reduced Order Modeling Framework for Flight Mechanics Oriented Modeling of On-Blade Control Concepts

Chengjian He and Jinggen Zhao

Advanced Rotorcraft Technology, Inc.
Mountain View, CA 94043, U.S.A.
he@flightlab.com

Jeremy Bain, Lakshmi Sankar, and J.V.R. Prasad
Georgia Institute of Technology
Atlanta, GA 30332, USA

Key words: reduced order airloads model, on-blade control

Abstract

The potential benefits of the application of modern on-blade control concepts such as variable camber, dynamic twist, and dynamic leading edge slat or trailing edge flap in rotor control have attracted increased interest. This paper discusses the development of a reduced order airloads model in support of flight mechanics oriented modeling of on-blade control concepts. The paper presents details of the formulated reduced order modeling framework that captures the essential dynamics and aerodynamics of various on-blade control concepts. The paper also presents sample evaluation results for an active trailing edge flap control simulated in FLIGHTLAB. The accuracy of the reduced order model (ROM) was validated against the CFD prediction from which the ROM was extracted. Excellent agreement was obtained including the complicated dynamic stall prediction, which substantiates the reduced order model formulation and NNET based model extraction technique.

1 Nomenclature

a	Speed of sound (ft/sec)
b	Semi-chord length, $c/2$ (ft)
b_δ	Semi-chord length for TE flap, $c_\delta/2$ (ft)
c	Chord length (ft)
c_δ	Chord length for TE flap (ft)

C_L, C_M, C_D	Airfoil lift, drag, and pitch moment coefficients, respectively
k	Reduced frequency for airfoil, $\omega b/V$ (non-dimensional)
k_δ	Reduced frequency for TE flap, $\omega_\delta b_\delta/V$ (non-dimensional)
LTI	Linear Time Invariant
M	Mach number, V/a (non-dimensional)
OBC	On-Blade Control
TE	Trailing Edge
V	Free stream velocity (ft/sec)
α	Airfoil angle-of-attack (deg)
$\dot{\alpha}$	Airfoil angle-of-attack rate (deg/sec)
α_0	Airfoil mean angle-of-attack (deg)
α_c	Airfoil cyclic angle-of-attack (deg)
δ_c	TE flap cyclic angle-of-attack (deg)
ω	Airfoil oscillatory frequency (rad/sec)
ω_δ	TE flap oscillatory frequency (rad/sec)
ψ_δ	TE flap phase angle (deg)
δ	OBC input (such as TE flap angle)
$\dot{\delta}$	Rate of change of OBC input

2 Introduction

Traditional swashplate controls in terms of collective and longitudinal and lateral cyclic limit the number of controls available to the control designer in addressing flight and rotor control issues, such as vibration and rotor noise. Individual Blade Control (IBC) and On-Blade Control (OBC) concepts offer potential for expanding the available control design space in tailoring control input signals for desired blade responses to address the flight control issues and rotor control issues in a unified framework. IBC and OBC concepts offer designers the potential to develop innovative controllers for mitigation of compressibility effects on advancing blades and reverse flow effects on retreating blades for improved rotor performance, control of an individual blade that may be off-track, mitigation of transient effects associated with rotor speed variations, mitigation of undesirable coupling between body and rotor in large size helicopters due to increased rotor blade flexibility, reduction of maneuver blade and rotor loads, reduction of vibratory hub loads, reduction of blade-vortex interaction noise, etc., while ensuring good flying qualities as specified in the Aeronautical Design Standard (ADS-33, Ref. [1]). While higher flight control bandwidth can be achieved through innovative integrated flight and rotor control designs, the implications of such higher bandwidth control arising out of IBC and OBC concepts on handling qualities and vehicle-pilot-biodynamic coupling, etc., need to be carefully assessed before they can be fully realized.

Research has been conducted on a range of on-blade control concepts including variable camber, dynamic twist, and dynamic leading edge slat or trailing edge flap (Refs. [2] to [8]). The state-of-the art CFD coupled with CSD analysis tools for assessing the implications of IBC and OBC concepts are computationally expensive and are not suitable for the controller synthesis, analysis, and simulation that is required in the design cycle. A need

exists for the development of reduced-order models that capture the essential physics of the impact of IBC and OBC concepts on rotor aerodynamics to fully realize the potential advantages offered by IBC and OBC concepts. This research explored the use of neural networks for arriving at reduced order models of various on-blade control concepts. The ROM thus derived was incorporated into the FLIGHTLAB simulation and tested for linear time invariant (LTI) model extraction in support of design and evaluation of both IBC and OBC concepts.

3 CFD Airloads Database of OBC Concepts

The development of reduced order models for selected OBC concepts was pursued with modern high fidelity CFD simulations that evaluate the the impact of selected OBC concepts on blade aerodynamics and create the airloads database accordingly. The airloads database for the OBC concepts in consideration was developed with properly selected model variables. The database thus generated is then used to extract the reduced order model (ROM) that will reflect the essential physical characteristics of the OBC concepts for rotorcraft flight mechanics and control applications. An enhanced OVERFLOW CFD tool was utilized for the airloads database development. The detailed discussion of the CFD numerical methodology and simulations can be found in Ref. [9]. A brief description is extracted here for reference.

The enhanced OVERFLOW Navier-Stokes CFD code was adopted for the on-blade concept simulation (Ref. [9]). The CFD simulations were performed for both 2D airfoils and 3D rotor blades. For the purpose of illustrating the ROM extraction process, only 2D airfoil data were used in the ROM construction and discussion. For the 2D airfoil airloads calculation, a C-grid was used. In order to adequately simulate the dynamic stall, 35,000 time steps per loop were used with multiple Newton sub-iterations (Ref. [10]). The CFD solution utilized 4th order central differencing and two turbulence models were evaluated. For the data generation, efforts were first made to validate the CFD simulation. Figure 1 shows sample results for the static and dynamic stall characteristics of the NACA 0012 airfoil. Comparisons with the results of McCroskey et. al. (Ref. [11]) are also shown. Between the two turbulence models employed, it was observed that the KES model captures the maximum lift of 1.29 at 13.4° that is within the experimental scatter. The Spalart-Allmaras (SA) model predicts a maximum lift of 1.43 at 14.8°. After the airfoil stalls, SA smoothly decreases while KES shows unsteady fluctuations associated with vortex shedding. Figure 2 compares the SA and KES results for the NACA 0012 for deep stall conditions. At low angles of attack, the two models have similar results as expected. The SA model overestimates the peak lift, drag, and pitching moment while the KES model does a significantly better job of predicting these critical quantities. In the CFD database generation for the current study, the KES turbulence model was used.

Figure 3 further shows the effect of the active flap. The simulation was conducted for an SC-1095 airfoil augmented with a trailing flap. The baseline airfoil was oscillating at an angle of attack of $\alpha = 10.0 + 8sin(\omega t)$ with $k = 0.05$ and $M = 0.3$. The TE flap profile is defined with a ramp up/down time of 1.05 (rad) at two amplitudes: -10.0 and -15.0 degrees (flap angle is positive down). As seen, the TE flap deflection reduced the maximum lift, drag, and pitching moment during the stall.

4 Reduced Order Model Formulation

The development of a reduced order model (ROM) was aimed at capturing the essential physics of the impact of selected OBC concepts on blade aerodynamics. A Neural Network (NNET) technique was adopted for the ROM derivation. Neural Networks, or artificial neural networks to be more precise, represent a technique that is rooted in many disciplines: neuroscience, mathematics, physics, computer science, and engineering (Ref. [12]). Neural networks find widespread applications in such diverse fields as modeling and data processing. A neural network, made up of an interconnection of nonlinear neurons, is itself nonlinear. Nonlinearity is a highly important property, particularly for mapping rotorcraft aerodynamics, which are inherently nonlinear.

For OBC applications, the reduced order airloads model is formulated as a superposition of a baseline airloads model and the incremental difference between the baseline and the CFD simulation. The baseline airloads model can be a conventional engineering model without the effects of OBC. The incremental difference or the delta airloads is derived by subtracting the CFD results from the baseline airloads model and formulated as a NNET presentation. The following summarizes the derivation of the ROM.

- Baseline airloads model:

$$[C_L\ C_M\ C_D]_{base} = f_{base}(\alpha, \dot{\alpha}, M) \tag{1}$$

- CFD data with OBC effects:

$$[C_L\ C_M\ C_D]_{cfd} = f_{cfd}(\alpha, \dot{\alpha}, M, \delta, \dot{\delta}) \tag{2}$$

- Difference between the CFD and the baseline:

$$\Delta[C_L\ C_M\ C_D]_{OBC} = [C_L\ C_M\ C_D]_{cfd} - [C_L\ C_M\ C_D]_{base} \tag{3}$$

- NNET approximation of $\Delta[C_L C_M C_D]_{OBC}$:

$$\Delta[C_L\ C_M\ C_D]_{nnet} = f_{nnet}(\alpha, \dot{\alpha}, M, \delta, \dot{\delta}) \tag{4}$$

- Reduced order model (ROM):

$$[C_L\ C_M\ C_D]_{ROM} = f_{nnet} + f_{base} \tag{5}$$

In the testing process, a FLIGHTLAB unsteady airfoil model was used as the baseline reference. The CFD simulation was performed for a range of α, $\dot{\alpha}$, M, δ, and $\dot{\delta}$. The delta airloads were then computed from the differences between the CFD and the baseline. Figure 4 illustrates the NNET formulation for the ROM that reflects the OBC effects.

The NNET model training is a very time consuming task. By organizing the lift, drag, and pitch moment coefficients into three individual NNET modules, it dramatically improved the NNET model training effort and accuracy at the same time.

5 CFD Test Matrix for Database Generation

The database for extracting the ROM is expressed in the form of airfoil load coefficients $[C_L\ C_M\ C_D]$ at different instantaneous parameters $[\alpha\ \dot{\alpha}\ \delta\ \dot{\delta}\ M]$, which will be convenient for the generation of the ROM using NNET. In addition, the pitching moment coefficient should be expressed at the airfoil quarter-chord position. Therefore, the data format for the CFD output should be as follows:

$$[\alpha\ \ \dot{\alpha}\ \ \delta\ \ \dot{\delta}\ \ M\ \ C_L\ \ C_D\ \ C_M]$$

where each column corresponds to a parameter and/or airload coefficient and each row corresponds to an instant in time.

A test matrix was carefully designed to carry out the CFD simulation in order to generate an airloads database adequate for generating the Reduced Order Model (ROM) using a Neural Network (NNET) for practical applications. To illustrate the process, the CFD simulation was mainly focused on the trailing edge (TE) flap device. In the CFD simulation, both the airfoil and TE flap angles-of-attack are expressed as sinusoidal signals as follows:

$$\alpha = \alpha_0 + \alpha_c\ sin(\omega\ t) \tag{6}$$

$$\delta = \delta_c\ sin(\omega_\delta\ t + \psi_\delta) \tag{7}$$

where the oscillation frequencies, ω and ω_δ, can be determined from the reduced frequencies as follows:

$$k = \frac{\omega b}{V} \tag{8}$$

$$k_\delta = \frac{\omega_\delta b_\delta}{V} \tag{9}$$

Assuming that the TE chord length $c_\delta = c/4$, a second TE flap harmonic control ($\omega_\delta = 2.0\,\omega$) will give a reduced frequency for the TE flap as $k_\delta = 0.5k$ and a fourth TE flap harmonic control ($\omega_\delta = 4.0\,\omega$) will give $k_\delta = 1.0k$, respectively.

For the database generation, three reduced frequencies, $k = 0.03, 0.05, 0.1$, were specified for the angle of attack change and two, $k = 0.5, 1$, were selected for the trailing edge flap angle variation. Three flap angle magnitudes, were simulated: 0, 4, and 7 degrees for the lower Mach numbers (M = 0.3 and 0.4); 0, 3, and 5 degrees for the medium Mach numbers (M = 0.5 and 0.6); and 0, 1.5, and 3 degrees for the high Mach number (M = 0.7). Each set of the trailing edge flap variations involves three phase angle changes: 0, 90, and 180 degrees. Almost 3,000 CFD runs need to be made in order to establish an adequate database for practical applications. Although the CFD computational effort is tremendous, the CFD database generation is only a one time task for each OBC configuration as given.

In the process of extracting the NNET model from the CFD database, it was found that the resolution of angle of attack for drag computation needs to be refined to as low as one degree if a high degree of accuracy is required. This requires a huge number of CFD case runs. The development of such a complete CFD database is beyond the goal of this research, which emphasizes the exploration the ROM concept and the illustration of the ROM derivation process. Therefore, it was decided that the data resolution gap would only be filled by using the data generated from a semi-empirical airfoil model.

6 Reduced Order Model Evaluation

The accuracy of the reduced order model was evaluated through comparisons with the CFD results from which the ROM was extracted. Sample results were shown in Figs. 5 and 6. Figure 5 compares the ROM prediction of the lift coefficient of an SC-1095 airfoil in a deep dynamic stall. The ROM result correlates well with the CFD simulation in terms of both trend and magnitude. The ROM prediction also closely follows the trend of the secondary oscillation of C_L during the early stage of the stall recovery as shown in the CFD results, but it is not as oscillatory as the CFD data. This could be improved by refining the NNET neuron structure. However, such a minor discrepancy is not a concern for practical applications. Similarly, good correlation of the pitch moment coefficient prediction by ROM with CFD was also achieved (Fig. 6).

7 Applications

The reduced order model provides a very computationally efficient tool for design and evaluation of advanced on-blade control concepts. The first effort toward the OBC design is the generation of constant coefficient linearized models that reflect the effect of OBC for integrated flight and rotor control studies. This is carried out in two steps. First, a linear time periodic (LTP) model with sufficient fidelity is extracted from a nonlinear model about a specified steady state flight condition using a numerical perturbation scheme. In the second step, the extracted LTP model is used to arrive at an approximate LTI model for the intended use of the model to a specific rotor control problem (Ref. [13]). For illustration, an example on-blade control using active trailing edge flap was evaluated. Figure 7 illustrates the testing example where the trailing edge flap was applied over a blade section from 0.55 to 0.91 of the rotor radius for a generic 4-bladed articulated rotor. The effect of OBC in terms of active trailing edge flap was first evaluated. For this, an example profile of the trailing edge flap was applied

$$\delta = 2sin(2\psi - 30^\circ) \tag{10}$$

Figure 8 shows the variation of the longitudinal rotor hub force under the excitation of the 2/rev active trailing flap as described in Eq. 10. Compared to the baseline without the active flap excitation, the effect of the on-blade control is apparent in the ROM simulation. Figures 9 and 10 show the variation of the lateral and normal rotor hub force components, respectively. A similar effect from OBC as presented in the ROM can be observed. The application of the active trailing edge flap with the second harmonic profile (Eq. 10) significantly reduces the oscillatory component of the hub shear force. Notice that the prescribed second harmonic active flap control is an estimated control for functional testing only, instead of an optimized one for overall rotor hub vibratory load reduction. In fact, this profile caused some increase in the hub moment components although it did reduce all the vibratory shear components.

The Linear Time Invariant (LTI) model derived for the testing case was also validated by comparison of the LTI results with the corresponding nonlinear simulation in FLIGHTLAB. Figure 11 shows the comparison results. Excellent agreement was obtained for all six components of the rotor hub forces and moments in terms of both magnitude

and variation frequencies. Further details of the ROM applications for integrated flight and rotor control can be found in Ref. [13].

8 Concluding Remarks

A reduced order airloads model based on a neural network was formulated for rotor on-blade control applications. The general procedures of constructing the reduced order model (ROM) was discussed and demonstrated via an active trailing edge flap example. The accuracy of the ROM was validated against the CFD simulation from which the ROM was derived. Excellent agreement was achieved. The application of the ROM was also illustrated through an integrated rotor control study.

9 Acknowledgments

This research was sponsored by NASA Cooperative Agreement NNX07AP33A, entitled "Flight Mechanics and Control Oriented Modeling for Next Generation On-Blade Control Concepts" with Dr. Wayne Johnson as the technical monitor. Dr. Johnson's very valuable feedback on the reduced order modeling approach is gratefully acknowledged.

References

[1] Anon., "*Handling Qualities Requirements for Military Rotorcraft, Performance Specification*," ADS-33E-PRF, USAAMC, Aviation Engineering Directorate, March 2000

[2] Straub, F. K. and Merkley, D. J., "Design of a Servo-Flap Rotor for Reduced Control Loads," Proceedings of the American Helicopter Society 50th Annual Forum, Washington, D.C. May 11-13, 1994

[3] Nitzsche, F. and Breitbach, E., "A Study on the Feasibility of Using Adaptive Structures in the Attenuation of Vibration Characteristics of Rotary Wings," Paper No. AIAA-92-2452, April 1992

[4] Marcolini, M.A, et. al., " Control of BVI Noise Using An Active Trailing Edge Flap," Proceedings of American Helicopter Society Vertical Lift Aircraft Design Conference, San Francisco, CA, Jan. 18-20, 1995

[5] Guzel, G.; Sankar, L.N.; and Rhee, M., "Computational Investigation of the Effects of Gurney Flap on the Aerodynamic Performance of VR-12 Airfoil," 23rd AIAA Applied Aerodynamics Conference, Toroton, Ontario, Canada, June, 2005

[6] Fulton, M., "Aeromechanics of the Active Elevon Rotor," Proceedings of the American Helicopter Society 61st Annual Forum, Grapevine, TX, June 2005

[7] Sahin, M.; Sankar, L.N.; Chandrasekhara, M.S.; and Tung, C., "Dynamic Stall Alleviation USing a Deformable Leading Edge Concept - A numerical Study," **Journal of Aircraft**, Vol. 40, No. 1, 2003

[8] Chandrasekhara, M.S.; Martin, P.B.; and Tung, C., "Compressible Dynamic Stall Control Using a Variable Droop Leading Edge Airfoil," 41th AIAA Aerospace Sciences Meeting and Exhibit, Reno, Nevada, January, 2003

[9] Bain, Jeremy J,; Sankar, L.N.; Prasad, J.V.R.; Bauchau, O.; Peters, D.A.; and He, Chengjian, "Computational Modeling of Variable-Droop Leading Edge in Forward Flight," **Journal of Aircraft**, Vol. 46, Issue, 2, April, 2009

[10] Bain, Jeremy J,; Mishra, S.; Sankar, L.N.; and Menon, S., "Assessment of a Kinetic-Eddy Simulation Turbulence Model for 3-D Unsteady Transonic Flow," 26th AIAA Applied Aerodynamics Conference, Honolulu, HI, AIAA-Paper 2008-7176, Aug. 2008

[11] McCroskey, W.; McAlister, Carr; Pucci, L., "An Experimental Study of Dynamic Stall on Advanced Airfoil Sections Volume 1-3, September 1982 NASA TM 84245

[12] Haykin, Simon, **Neural Networks**, 2nd edition, Prentice Hall, 1999

[13] Prasad, J.V.R.; Olcer, F.E.; Sankar, L.N.; and He, Chengjian, "Linear Time Invariant (LTI) Models for Integrated Flight and Rotor Control," 35^{th} European Rotorcraft Forum, Hamburg, Germany, Sept. 2009

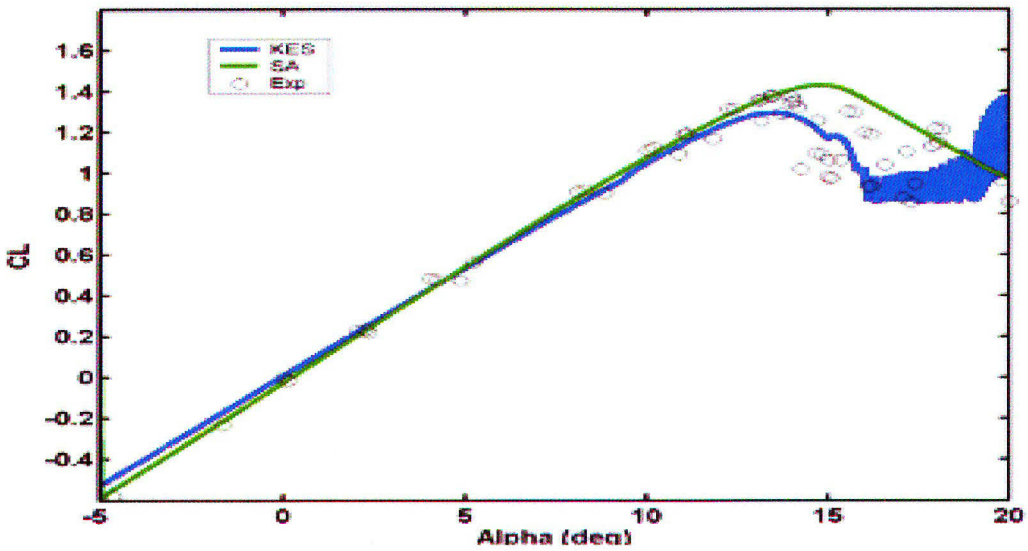

Figure 1: CFD prediction of static NACA0012 lift coefficient

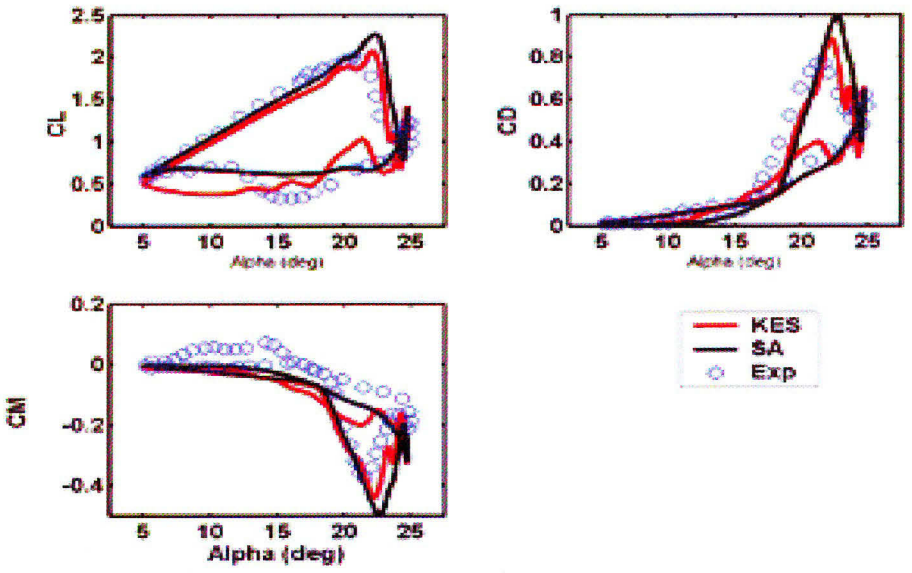

Figure 2: CFD simulation of NACA0012 dynamic stall ($M = 0.3, k = 0.1, \alpha = 15° + 10° sin(\omega t)$)

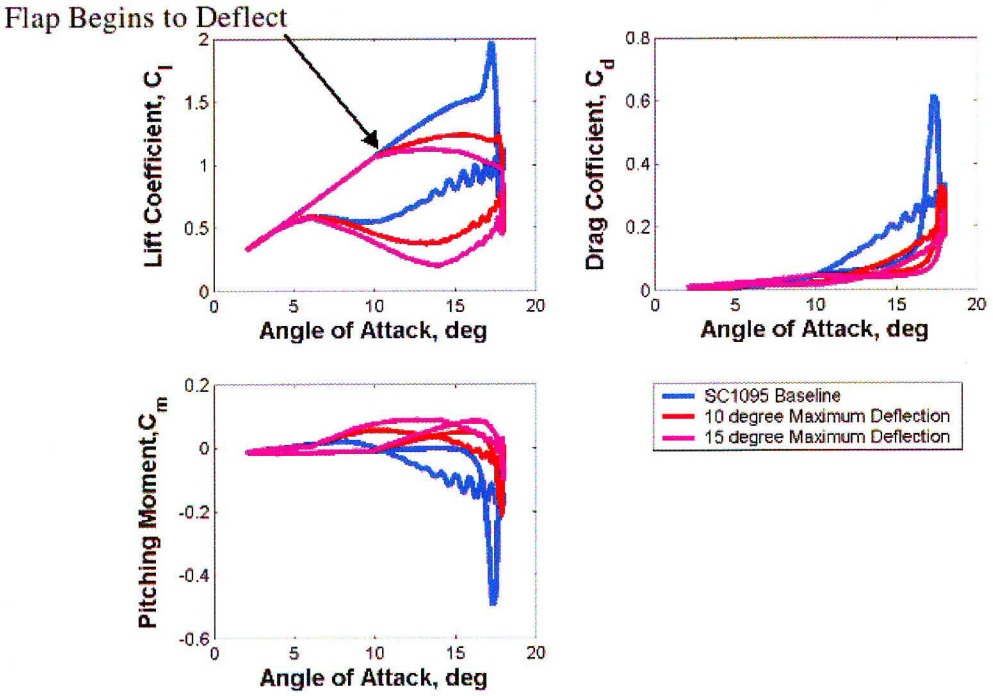

Figure 3: CFD simulation of active TE flap

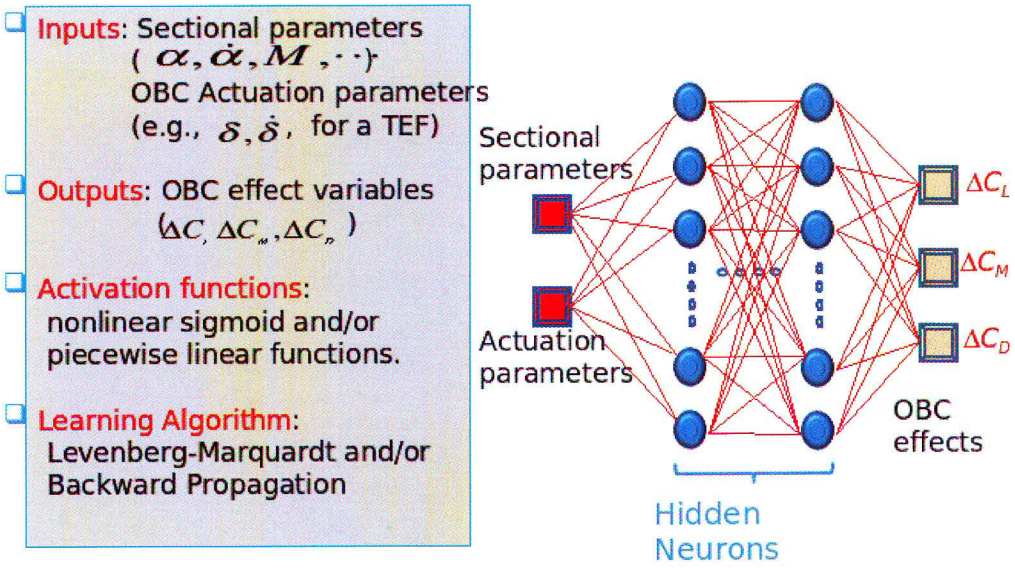

Figure 4: NNET framework for ROM

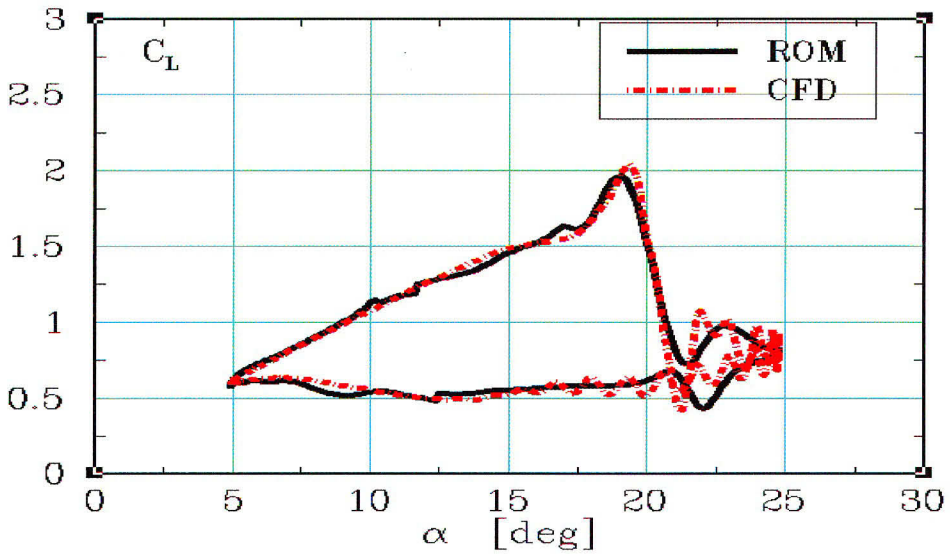

Figure 5: Comparison of ROM prediction with CFD simulation (lift coefficient)

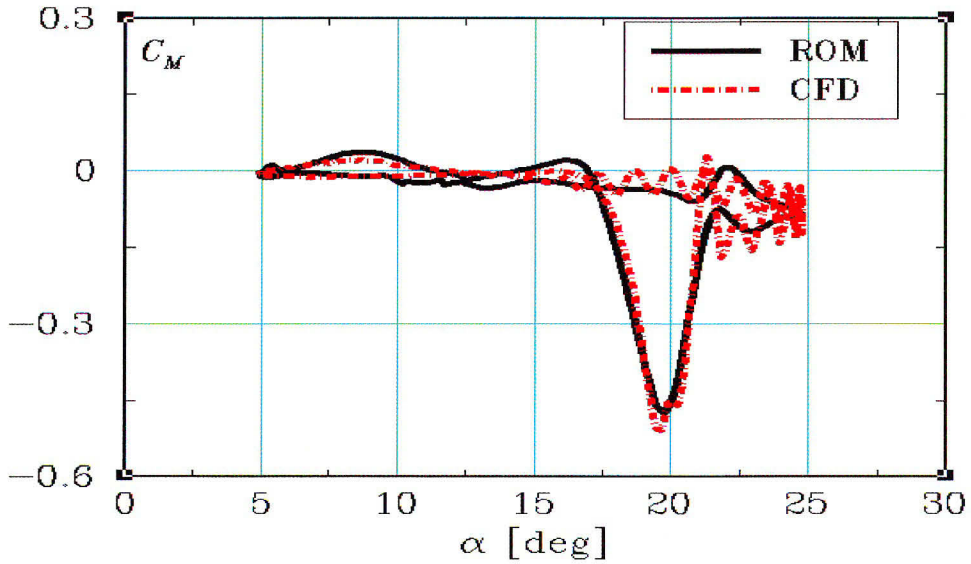

Figure 6: Comparison of ROM prediction with CFD simulation (pitch moment coefficient)

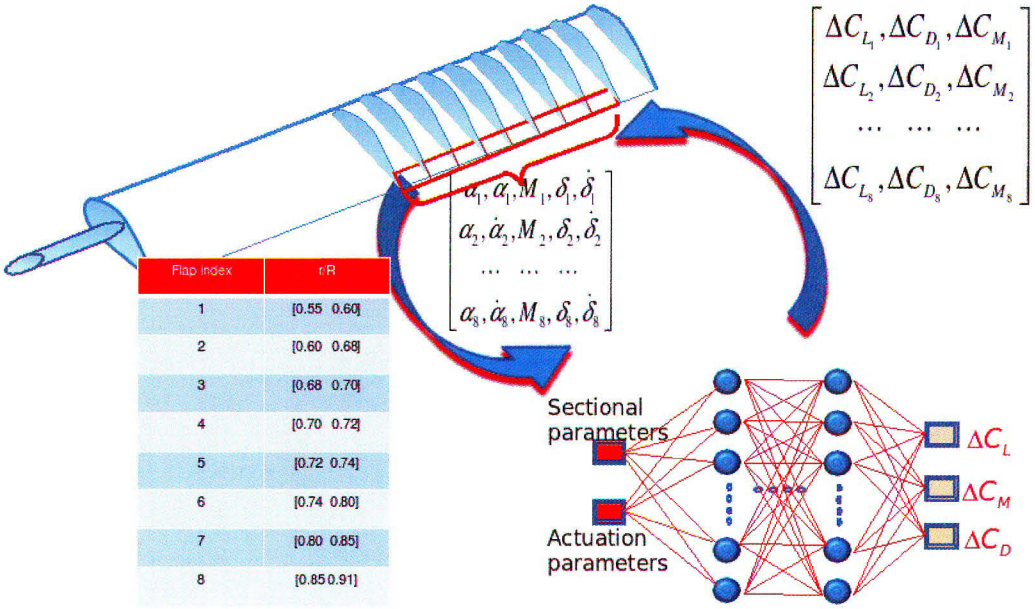

Figure 7: Implementation of ROM for active trailing flap control studies

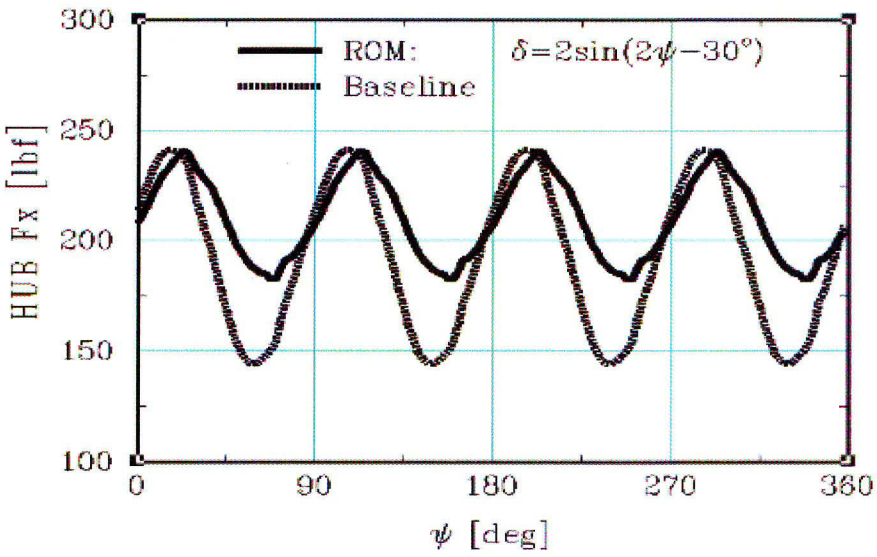

Figure 8: Effect of active trailing flap on rotor hub force (F_x)

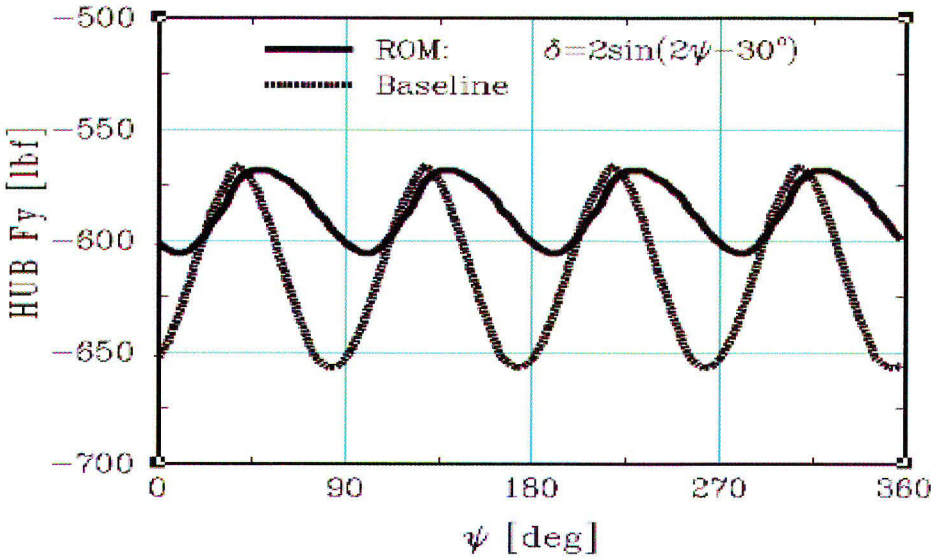

Figure 9: Effect of active trailing flap on rotor hub force (F_y)

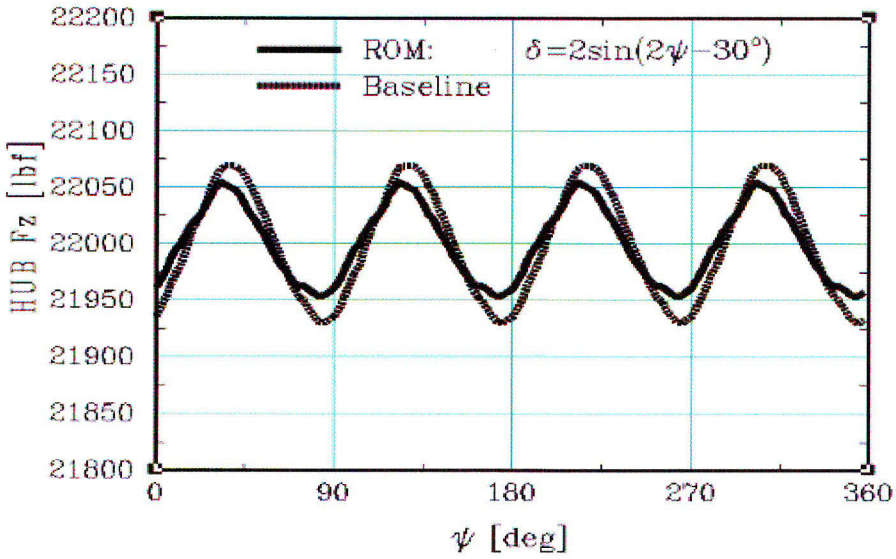

Figure 10: Effect of active trailing flap on rotor hub force (F_z)

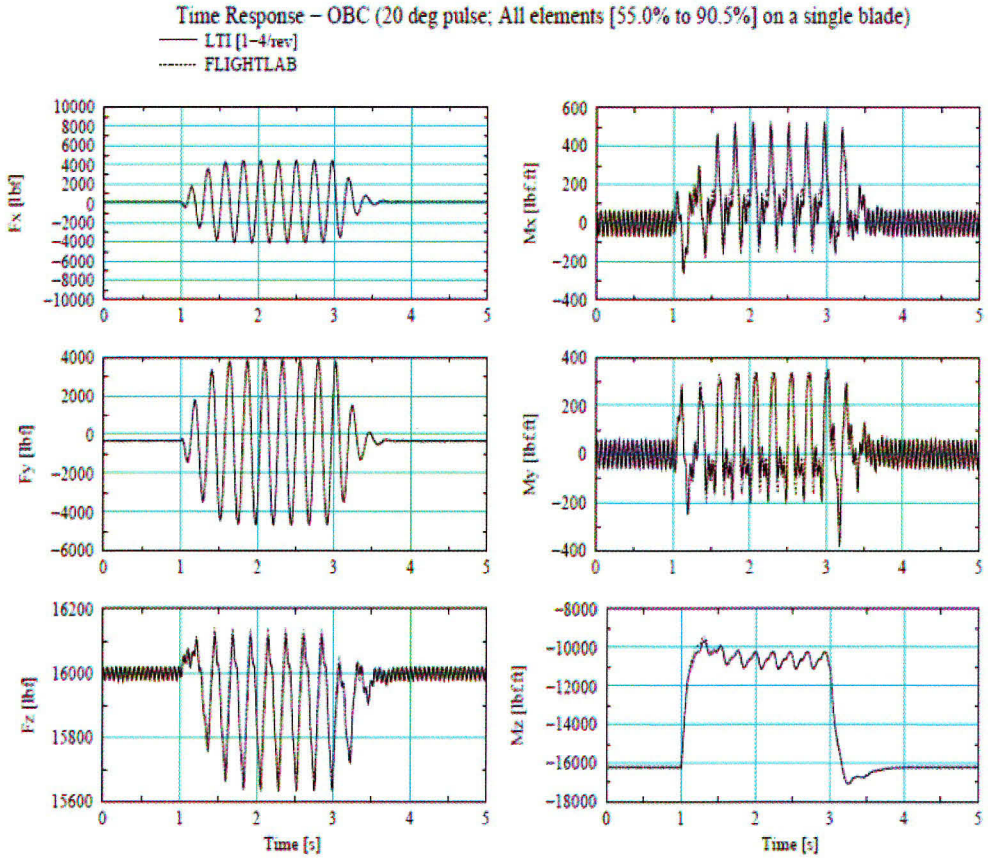

Figure 11: Comparison of the LTI model with nonlinear simulation in FLIGHTLAB